Sedimentologika

10.57035/journals/sdk.2026.e41.1937

Settling velocity of sediment grains, Part 1: Natural sediment particles are not ellipsoids

Arnoud Slootman* [1,2], **Max de Kruijf** [3], **Guenther Glatz** [4], **Joris T. Eggenhuisen** [5], **Zane R. Jobe** [1], and **John J.G. Reijmer** [6]

[1]Department of Geology and Geological Engineering, Colorado School of Mines, Golden, CO, USA
[2]Division of Earth and Planetary Sciences, Graduate School of Science, Kyoto University, Kyoto, Japan
[3]TNO – Geological Survey of the Netherlands, Utrecht, The Netherlands
[4]Chemical & Petroleum Engineering, The University of Kansas, Lawrence, KS, USA
[5]Department of Earth Sciences, Utrecht University, Utrecht, The Netherlands
[6]Department of Earth Sciences, Faculty of Science, Vrije Universiteit Amsterdam, Amsterdam, The Netherlands

CRediT statement: *Writing-original draft*: AS, MdK. *Writing-review & editing*: JTE, JJGR, ZRJ. *Visualization*: AS, GG. *Conceptualization*: AS, MdK, JJGR. *Data curation*: AS, MdK, GG. *Formal analysis*: AS, MdK, GG. *Investigation*: AS, MdK, GG, JJGR. *Methodology*: AS, MdK. *Software*: AS, GG. *Resources*: AS, JTE, JJGR. *Validation*: AS, MdK, GG. *Supervision*: JJGR. *Funding acquisition*: JJGR, ZRJ.

*Corresponding author: Arnoud Slootman, arnoudslootman@gmail.com

Abstract

Particle settling velocity has wide application in sedimentology and engineering. The ability to predict settling velocity based on fluid and particle properties is essential for realistic sediment transport models. It is common practice to describe the size and shape of natural sediment grains with an ellipsoidal model. This paper tests the validity of the ellipsoidal model for predicting particle settling velocity for siliciclastic and carbonate sediments. The parameters associated with this model are the ellipsoidal nominal diameter $\left(D_n = \sqrt[3]{D_s D_i D_l}\right)$ and Corey shape factor $\left(CSF = D_s/\sqrt{D_i D_l}\right)$, calculated from the short (D_s), intermediate (D_i), and long (D_l) axial diameters. An equation for the drag coefficient (i.e., nondimensional friction) expressed as a function of particle Reynolds number (i.e., nondimensional particle size) and Corey shape factor (i.e., ellipsoidity) was reconstructed for siliciclastic and carbonate grains separately, based on the largest available compilations of existing datasets (639 siliciclastic and 3 666 carbonate grains). The ellipsoidal approximation of grain size yields significant errors in settling velocity predictions, yet the equation is more accurate for siliciclastic particles (mean absolute error = 14 %) than for carbonate grains (mean absolute error = 21 %). This difference is explained by the enlarged irregularity of particles in carbonate compared to siliciclastic sediments, due to enhanced angularity and surface roughness of skeletal remains. Thus, the ellipsoidal model, using the nominal diameter and Corey shape factor, is not suitable for describing natural sediments or predicting their settling velocity, despite its widespread use. A companion paper (*Part 2*, Slootman et al., 2026) investigates alternative particle size and shape descriptors.

Research Article

Executive Editor
Murray Gingras

Associate Editor
Siddhi Josh

Reviewers
Yuhao Li
Urs Neumeier
One anonymous reviewer

Production Manager
Jarred Lloyd

Copy Editor
Seyedeh Mortazavi

Received: 2025-04-24
Accepted: 2025-07-18
Published: 2026-03-26

Keywords
settling velocity
grain size
particle shape
Reynolds number
drag coefficient

Plain language summary

The speed at which sediment grains fall through water (settling velocity) reveals how much friction occurs between the fluid and the grain, which contributes to the understanding of sediment transport dynamics. Sediment particles are usually modelled as ellipsoids. This paper has compiled datasets containing the settling velocity, density, size, and ellipsoidity of thousands of sediment grains from the two main groups of sediment composition: siliciclastic and carbonate. Relationships between these variables were investigated to derive an equation for predicting settling velocity. The ellipsoidal model cannot accurately predict settling velocity because natural sediment grains have irregular shapes, such as sharp corners and rough surfaces, causing friction not captured by the model. However, fall velocity can be predicted more accurately and more precisely for siliciclastic particles than for carbonate grains as a result of the irregular nature of skeletal remains such as corals and shells compared to rounder and smoother quartz particles. We conclude that ellipsoids do not offer the best geometric representation of natural sediments.

1 Introduction

Settling velocity is a fundamental parameter in sedimentology (Dey et al., 2019; Le Roux, 2005), essential to hydrodynamic modelling of sediment threshold conditions of bedload and suspended load transport (Camenen et al., 2006; Collins & Rigler, 1982; Dey & Ali, 2019). For example, settling velocity has a control on erosion criteria (see Egiazaroff, 1965; and Hjulström, 1935; in Miedema, 2010). Settling velocity equations have applications in transport models for natural sediment grains in lakes and oceans (Ganti et al., 2014; Lamb et al., 2010; Mulder & Alexander, 2001), rivers (Cassel et al., 2021) and the atmosphere (Poulidis et al., 2021), but are also relevant to processes in magma chambers (Martin & Nokes, 1988), mining engineering (Walsh & Rao, 1988), civil engineering (Ghoddousi et al., 2014), botany (Zhu et al., 2017), meteorology (Cheng et al., 2014), food industry (McKay et al., 1989) and sewage treatment (Polorigni et al., 2021).

Settling velocity dynamics of spherical particles are well constrained (Clift & Gauvin, 1971). However, sediment grains rarely ever are spheres (Barrett, 1980; Griffiths, 1967; Schulz et al., 1954). In particular, carbonate grains composed of skeletal remains of organisms commonly possess irregular shapes (Figure 1A; Braithwaite, 1973; Maiklem, 1968; Musso et al., 2025; Slootman et al., 2023). An ellipsoidal particle model, with short, intermediate and long axes (D_s, D_i, D_l), is commonly applied to approximate non-spherical grains (Figure 1B; Baba & Komar, 1981; Blott & Pye, 2008; Komar & Reimers, 1978; Krumbein, 1941; Smith & Cheung, 2003). A particle diameter used to represent the size of non-spherical grains is the equivalent diameter (Wadell, 1932), which is the diameter of a sphere (i.e., the equivalent sphere) with the volume V of the non-spherical particle: $D_{eq} = \sqrt[3]{6V/\pi}$. In the ellipsoidal model, the equivalent diameter is approximated by the volume of an ellipsoid to calculate the nominal diameter: $D_n = \sqrt[3]{D_s D_i D_l}$.

In addition to particle size, settling velocity equations for non-spherical grains typically prompt the introduction of a shape factor to account for the influence of particle shape, such as the widely applied Corey (1949) shape factor: $CSF = D_s/\sqrt{D_i D_l}$. This shape factor constitutes a measure of ellipsoidity as a first-order approximation of particle shape (i.e., particle form). Second-order shape properties (i.e., angularity or roundness) and third-order shape properties (i.e., surface texture) are not accounted for by the Corey shape factor (Barrett, 1980; Griffiths, 1967). Although CSF cannot discriminate between ellipsoids in the flatness-elongation diagram of Zingg (1935) (Figure 1C), the Corey shape factor does provide a measure of the particle's maximum projection area (De Kruijf et al., 2021, Figure 14). Particles fall perpendicular to their maximum projection area (Clift et al., 1978; Stringham et al., 1969), which therefore exerts an influence on the magnitude of the settling velocity for which CSF thus offers an indication.

Two companion papers investigate the settling velocity of natural sediment grains. The aim of this paper (*Part 1*) is to examine the validity of the ellipsoidal particle model in settling velocity problems. The appropriateness of the widely used nominal diameter to represent grain size, and the Corey shape factor to describe grain shape in settling velocity equations is tested. These parameters are evaluated using the two most common sediment compositions: siliciclastic and carbonate. The companion paper (*Part 2,* Slootman et

al., 2026) explores alternative measures of particle size and shape.

Nearly all types of natural sediment grains are non-spherical (Barrett, 1980; Griffiths, 1967; Schulz et al., 1954). However, only a small number of the giant pool of published settling velocity experiments document the ortho-axial dimensions of the tested particles, which are required for the computation of the ellipsoidal nominal diameter and Corey shape factor. The scarcity of reported shape data is notable, given the abundance of literature on the topic of settling velocity. The available datasets that do contain shape information, however, have limited ranges of investigated particle size, and may be exclusive to sediment in a specific environment. For the first time, all datasets available from the literature are here combined into the two largest compilations to date of experimental settling results of individual sediment grains with known principal axes. The siliciclastic compilation contains 13 datasets with 639 particles, and the carbonate compilation comprises 7 datasets with 3 666 particles. These are used to test the validity of the nominal diameter and Corey shape factor, i.e., the ellipsoidal particle model, as descriptors of particle size and shape to predict settling velocity.

2 Nondimensional settling velocity equations

Nondimensionalisation of settling velocity equations, i.e., the removal of physical dimensions and their units, intends to make equations independent of quantitative measurements (e.g., Middleton & Southard, 1984; Southard, 2006). A nondimensional equation is equally applicable to different compositions and shapes. If that is not the case, then one or more of these parameters are either inappropriate or incomplete. The parameters relevant to the settling velocity of a sediment grain falling vertically through a fluid follow from a consideration of the forces acting on the particle (see course notes by Middleton & Southard, 1984; and Southard, 2006). The downward force is the submerged weight $F_G{}'$ of the particle, i.e., the net force between the downward force of gravity and the upward buoyant force equal to the weight of displaced water:

$$F_G{}' = g\left(\rho_p - \rho_f\right) V \tag{1}$$

where g is gravitational acceleration, ρ_p and ρ_f are densities of the particle and fluid, and V is particle volume. The submerged weight causes the particle to accelerate once it starts sinking upon release into the fluid. The opposing force is the drag force that results from friction between the particle and the fluid. There is no drag force if the particle is not moving. At low speeds, the drag force is dominated by skin friction, caused by adhesive forces between the particle surface and the fluid. In the case of laminar flow, the drag force for spheres is given by the law of Stokes (1850). Particles that fall faster generate fluid turbulence resulting in a pressure drop behind the particle, which acts on the particle as an upward resisting force. The drag force is usually formulated as a function of the dimensionless drag coefficient C_D, fluid density ρ_f, characteristic area A, and settling velocity w:

$$F_D = \frac{1}{2} C_D\, \rho_f\, A\, w^2 \tag{2}$$

With increasing fall velocity, the friction becomes progressively dominated by pressure drag (form drag). As the particle accelerates, the combination of skin friction and pressure drag grows until it equals submerged particle weight. At this point, there no longer is a resultant downward force to accelerate the particle, and terminal settling velocity w_t has been reached. Solving $F_G{}' = F_D$ for terminal settling velocity of a particle with nominal diameter D_n yields:

$$w_t = \sqrt{\frac{4}{3} D_n\, g \left(\frac{\rho_p}{\rho_f} - 1\right) \frac{1}{C_D}} \tag{3}$$

However, the drag coefficient is not constant and is a function of the particle Reynolds number Re_p:

$$C_D = f\left(Re_p\right) \tag{4}$$

The particle Reynolds number is a dimensionless length scale that represents the ratio of inertia to viscous fluid forces acting on the particle:

$$Re_p = \frac{D_n\, w_t}{\vartheta} \tag{5}$$

where ϑ is kinematic fluid viscosity ($\vartheta = \mu/\rho_f$, where μ is dynamic fluid viscosity, a measure of how 'thick' the fluid is). The two regimes (Figure 2), i.e., the regime dominated by skin-friction and the regime in which pressure drag is dominant, are respectively referred to as laminar or Stokesian (fluid flow in parallel layers) and turbulent or Newtonian (chaotic changes in pressure and velocity). These end-member regimes are separated by a transitional regime, in which a combination of skin friction and pressure forces operates.

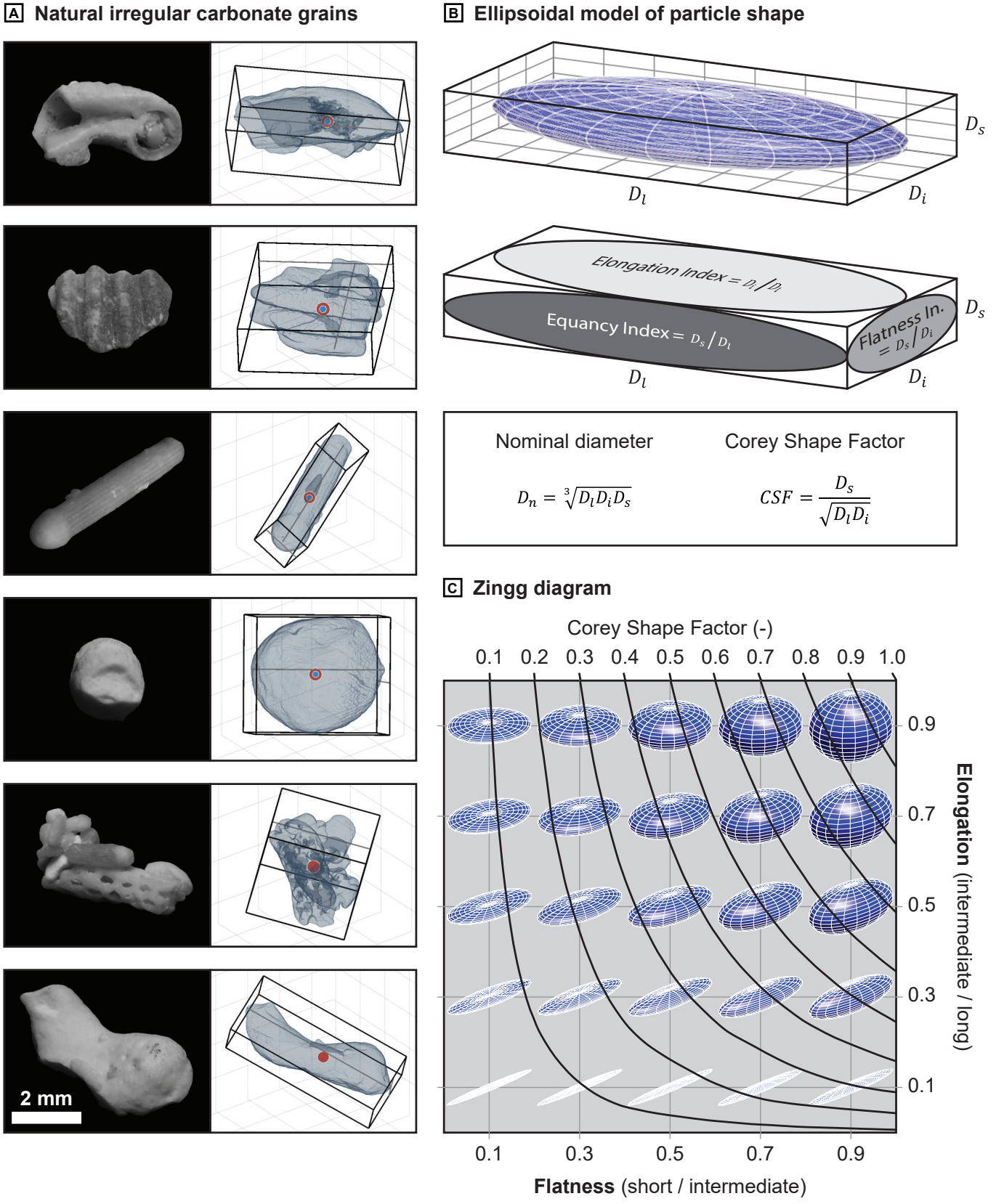

Figure 1 – **(A)** The size and shape of sediment particles is approximated with an ellipsoidal model. **(B)** The three principal axes of the ellipsoid are used to calculate nominal diameter and Corey shape factor. **(C)** The Zingg (1935) diagram is a common visualisation method for ellipsoidity. Corey Shape Factor isolines are shown. Adapted from Slootman et al. (2023).

Table 1 – Datasets in the compilations of **(A)** carbonate and **(B)** siliciclastic settling experiments of individual sediment grains.

Authors	Publication year	Sediment type	Specification	Grain measurement method	Data availability	Data points	Settling velocity	Three principal axes reported	Particle mass	Volume	Particle density	Fluid density	Viscosity	Measured maximum projection area
(A) Siliciclastic (*N* = 13, *n* = 639)														
Corey	1949	Fluvial[1]	River bed material (quartz, feldspar)	Microscope, fluid displacement	Paper[a]	49	Yes[b]	Yes	Yes	Yes	Single value	Yes	Single value	No
Corey	1949	Fluvial[2]	River bed material (quartz, feldspar)	Microscope, fluid displacement	Paper[a]	50	Yes[b]	Yes	Yes	Yes	Single value	Yes	Single value	No
Wilde	1952	Fluvial	River bed material (quartz, feldspar)[c]	Microscope, fluid displacement	Paper[a]	50	Yes[b]	Yes	No	Yes	Single value	Yes	Single value	No
Schulz	1954	Fluvial	River bed material (quartz, chalcedony, feldpar)	Microscope, fluid displacement	Paper[a]	40	Yes[b]	Yes	No	Yes	Single value	Yes	Single value	No
Corey	1949	Aeolian	Wind-blown sand dune (quartz, feldspar)	Microscope, fluid displacement	Paper[a]	62	Yes	Yes	Yes	Yes	Yes	Single value	Yes	Yes
Wilde	1952	Glacial	Lateral moraine (quartz, feldspar)[c]	Microscope, fluid displacement	Paper[a]	50	Yes	Yes	No	Yes	Yes	Single value	Yes	Yes
Wilde	1952	Gravel stockpile	Unspecified source (quartz, feldspar)[c]	Microscope, fluid displacement	Paper[a]	39	Yes	Yes	No	Yes	Yes	Single value	Yes	Yes
Corey	1949	Rock crusher	Unspecified source (quartz, feldspar)	Microscope, fluid displacement	Paper[a]	39	Yes	Yes	Yes	Yes	Yes	Single value	Yes	Yes
Wilde	1952	Rock crusher	Unspecified source (quartz, feldspar)[c]	Microscope, fluid displacement	Paper[a]	87	Yes	Yes	No	Yes	Yes	Single value	Yes	No
Schulz	1954	Rock crusher	Unspecified source (quartz)	Microscope, fluid displacement	Paper[a]	28	Yes	Yes	No	Yes	Yes	Single value	Yes	No
Schulz	1954	Rock crusher	Unspecified source (feldspar)	Microscope, fluid displacement	Paper[a]	13	Yes	Yes	No	Yes	Yes	Single value	Yes	No
Goossens	1987a	Not specified	Unspecified source (quartz)	Microscope, mass conversion to obtain volume	Paper	92	Yes	Yes	Yes[d]	Yes	Single value[e]	Single value[e]	Single value[e]	Yes
Riazi & Türker	2019	Not specified	Unspecified source	Pseudo 3D stereographs	Paper	40	Yes	Yes	No	No	Yes	Yes	No	No
(B) Carbonate (*N* = 7, *n* = 3 666)														
Smith & Cheung	2003	Tropical	Beach (swash zone)	Microscope	Not published[f]	998	Yes	Yes	No	No	Single value	Single value	Single value	No
Alcérreca et al.	2013	Tropical	Beach (multiple zones)	Micropscope, image analysis	Not published[f]	1 557	Yes	Yes	No	No	Multiple single values	Single value	Single value	Yes
Wang et al.	2018	Tropical	Reef	Stereomicroscope, image analysis	Not published[f]	117	Yes	Yes	Yes	Yes	Yes	Yes	Yes	No
Li et al.	2019	Tropical	Lagoon	Digital image analysis, caliper	Supplementary materials	320	Yes	Yes	Yes	Yes[g]	Single value	Single value	Single value	Yes
Mao et al.	2023	Tropical	Aquarium sand	Image analysis of two faces	Supplementary materials	272	Yes	Yes	No	Unclear	Two single values	Single value	Single value	Yes
		Tropical	Coral debris	Image analysis of two faces	Supplementary materials	199	Yes	Yes	No	Unclear	Yes[h]	Single value	Single value	Yes
Slootman et al.	2023	Cool-water	Subaqueous dunes	Micro-CT	Supplementary materials	203	Yes	Yes	Yes	Yes	Yes	Yes	Yes	Yes

[1]Cache la Poudre River, near Bellevue, Colorado, USA. [2]Middle Loop River, Dunning, Nebraska, USA.
[a]Thesis results: compiled in Schulz et al., (1954). [b]Calculated from reported particle Reynolds number. [c]Not specified, but reported densities correspond with quartz and feldspar composition. [d]Measured, but not reported. [e]Assumed a single value based on text; actual value not reported. [f]Provided by authors. [g]Calculated from mass and particle density. [h]Calculated from reported particle-fluid density contrast.

Settling velocity experiments essentially aim to find a solution to the drag coefficient as a function of particle Reynolds number (Equation 4, red curve in Figure 2). This equation can be solved analytically for low particle Reynolds numbers in the laminar regime, for spheres known as Stokes' Law: $C_D = 24/Re_p$ (Stokes, 1850). However, for more turbulent conditions at higher particle Reynolds numbers, this equation must be solved empirically (Wadell, 1934). A widely accepted equation for spheres settling in the transitional regime is the equation of Clift & Gauvin (1971) (Equation A1 in Appendix A). Several studies looked into these relationships for non-spherical particles from a variety of depositional environments, with sediment types including siliciclastics, carbonates, volcaniclastics, heavy minerals, and plastics (e.g., Alger, 1964; Allen, 1984; Briggs et al., 1962; Francalanci et al., 2021; Goossens, 1987a; Joshi et al., 2014; Komar & Reimers, 1978; Li et al., 2020; Mao et al., 2023; Olivera & Wood, 1997; Riazi & Türker, 2019; Rouse, 1949; Smith & Cheung, 2003).

These equations are nondimensional, i.e., they are independent of the quantitative measurements of the system, enabling the results from settling experiments to be applied to settling problems with particles of different size, density and shape than tested in the experiments. Nondimensionalisation of relationships between settling velocity, and particle and fluid properties thus makes experimental results more generally applicable, rather than being limited to a single grain population from a specific depositional setting or composition. This also implies that fluids other than water may be used in experiments (e.g., oil or glycerine; Fan et al., 2022; Komar, 1980; Komar & Reimers, 1978; Stringham et al., 1969; Wang et al., 2018; Wilde, 1952). However, the success of nondimensional equations depends on the ability of parameters to properly capture the relevant particle properties of size, density and shape, as evaluated in this paper.

3 Compilations

3.1 Datasets

An extensive literature survey yields the most complete compilations of experimental results of siliciclastic and carbonate settling velocity to date (Table 1). Prerequisites for data to be incorporated into the compilations include reporting of settling velocity, the individual short, intermediate and long particle axes, grain density, and fluid density and viscosity. For fluid properties in particular, several studies report a single value, which may reflect constant laboratory conditions (e.g., dependent on temperature, and whether fresh or salt water was used). More experiments than reported here have been performed, however some of these could not be included in the compilations because the short, intermediate, and long axial dimensions were measured but not documented (e.g., Baba & Komar, 1981).

It must be stressed that these datasets do not necessarily represent natural sample populations, as most grains have been selected to represent a broad range of particle properties. This selection bias, however, is not relevant to the objectives of the present study, which aims to collect an as wide as possible range of particle properties of siliciclastic and carbonate composition. There is extreme variation in the number of investigated grains between datasets, ranging from about 40 to several hundreds, and in two cases about a thousand or more. For a visual overview of the distributions of grain size, density, shape and settling velocity, normal gamma probability density functions (Vaz & Fortes, 1988), grouped by composition, are shown in Figure 3.

For siliciclastics, a total of thirteen datasets with 639 particles were collected from a number of studies (Corey, 1949; Schulz, 1954; Wilde, 1952, as compiled in Schulz et al., 1954). Note that for some particles not all parameters were measured, hence total dataset size (N in figures) may differ between analyses. The siliciclastic compilation contains a variety of natural sediments collected from a range of depositional environments (fluvial, aeolian, glacial). To mimic conditions of freshly fragmented sediment, rock crusher products were included in the compilation of Schulz et al. (1954). In some of these datasets, individual mineral grains were specified. Riazi & Türker (2019) provide the only recent siliciclastic dataset that meets the requirements, covering an extreme range of particle densities from 1.56 to 4.43 mg mm^{-3}, but did not specify sediment source or composition.

For carbonates, a total of seven datasets with 3 666 particles were collected from six studies, all published in the twenty-first century. Two studies together comprise more than half of the data points. The carbonate datasets comprise a number of depositional environments, yet most grains were produced in tropical factories (sensu Schlager, 2003;

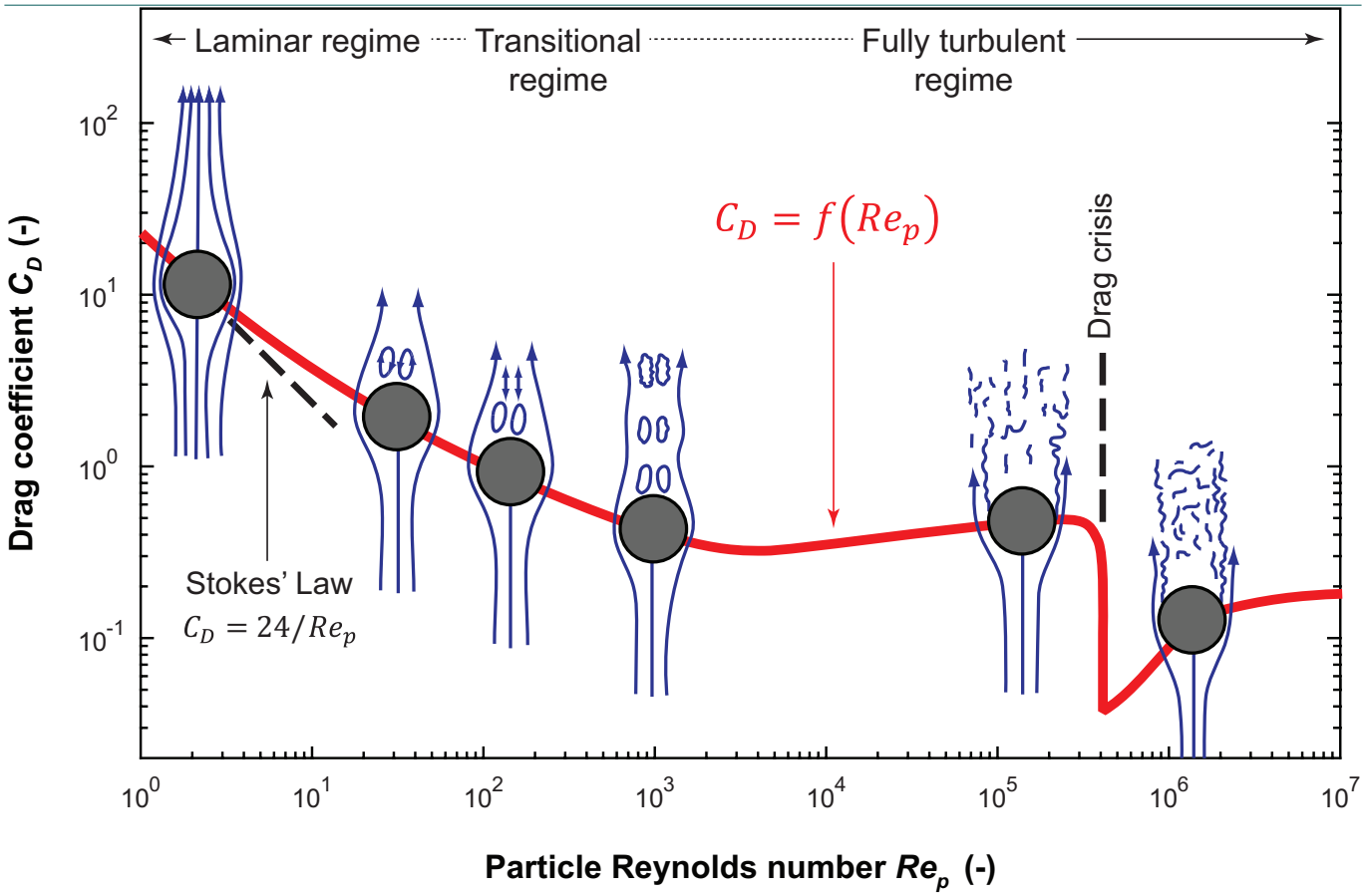

Figure 2 – Particle hydrodynamics as function of two nondimensional parameters: (1) Re_p: particle Reynolds number, a dimensionless length scale obtained by the ratio of inertial forces to viscous forces, and (2) C_D: drag coefficient, the ratio of drag force to dynamic pressure forces. Viscous forces dominate in laminar flow in the Stokesian realm. Inertial forces control turbulent flow in the Newtonian realm. The upper boundary of the laminar regime is placed at $Re_p = 10^{-1}$ (e.g., Bagheri & Bonadonna, 2016) to $Re_p = 10^0$ (e.g., Dey et al., 2019). Most sedimentary processes occur in the transitional regime up to $Re_p = 10^3$, proposed to be stretched to larger particle Reynolds numbers for irregular grain shapes (Smith & Cheung, 2003). The displayed $Re_p - C_D$ curve is from (Fornberg, 1988). Flow patterns are modified from MIT OpenCourseWare in (Southard, 2006). Figure adapted from De Kruijf et al. (2021).

as used in Reijmer, 2021). About half the data have not been published previously but were obtained from the authors upon request. Several of the carbonate studies report single values for particle density, which is peculiar given the wide range of published carbonate particle densities (see compilation in De Kruijf et al., 2021).

3.2 Parameters

In this section, the parameters required for calculation of the particle Reynolds number and drag coefficient are discussed (Figure 3). Some general, and remarkable, characteristics of the datasets are mentioned here.

3.2.1 Grain size

The nominal diameter was calculated using the reported short, intermediate and long particle axes, according to the ellipsoidal model: $D_n = \sqrt[3]{D_s D_i D_l}$. The classical datasets utilized microscopes to determine particle axes, as did some of the modern studies (Table 1). Other methods include three-dimensional stereographical techniques. However, digital image analysis is used most frequently. Only one study obtained particle dimensions from digital models constructed from micro-CT scans. The width of the grain-size distributions of the siliciclastic and carbonate compilations is approximately eight phi units (Krumbein, 1938; Wentworth, 1922). Yet, the siliciclastic compilation (medium sand to very coarse pebbles) contains particles that are up to two phi units coarser than in the carbonate compilation (very fine sand to medium pebbles).

3.2.2 Particle density

It is the density of the grain including fluid-filled macro-porosity that is relevant to the settling problem. Thus, it is not the solid material density that is

of interest here (see De Kruijf et al., 2021 for a discussion and review of carbonate particle densities). Siliciclastic particles can be assumed to be void of intraparticle macro-porosity. Siliciclastic particle volume is classically determined by submerging an individual grain into a serological pipette containing a known fluid volume (Corey, 1949; Schulz et al., 1954; Wilde, 1952). The volume displaced within the pipette equals the siliciclastic particle volume. In combination with the measurement of particle mass on an accurate and precise balance, particle density is then determined for siliciclastic grains. For the quartz and feldspar grains collected from riverbeds, single values for the well-constrained mineral densities were reported. For carbonate particles, the pipette method only works if carbonate grains do not contain intraparticle macro-porosity, such as bivalve fragments (Li et al., 2020). Yet, due to organism-specific micro-porosity in the crystal structure of carbonate skeletons (see Caromel et al., 2014; Yordanova & Hohenegger, 2007), it may be problematic to apply a single value for the density of the carbonate mineral (e.g., aragonite or calcite). For the datasets of Mao et al. (2023) it is unclear how fluid-filled macro-porosity was compensated for. An alternative approach to determine particle density of carbonate particles with fluid-filled macro-porosity is the method of Slootman et al. (2023), which separates the convex hull volume into the volumes of the intraparticle pore space and the solid material using micro-CT data, and then proportionally attributes the densities of respectively the fluid and the carbonate mineral (obtained from X-ray attenuation) to these volumes.

3.2.3 Particle shape

Particle shape is parameterized using the Corey shape factor (Blott & Pye, 2008; Corey, 1949), based on the short, intermediate and long diameters of the grain: $CSF = D_s/\sqrt{D_i D_l}$. Both siliciclastic and carbonate datasets attain broad shape distributions. Perhaps counterintuitively, the siliciclastic datasets contain very non-spheroidal particles, likely as a result of selection bias. The bivalve fragments from Li et al. (2020) are extremely flat. The wide distribution of particle shape is apparent when data points are plotted in the flatness-elongation diagram of Zingg (1935) (Figure 3, see also Figure 1C).

3.2.4 Settling velocity

Reported settling velocities were obtained from experiments by releasing sediment particles in transparent tubes, and averaging the ratios of a known vertical distance between markers over the recorded times needed to pass those markers. Several fluids were used in the experiments; however, Figure 3 displays only the settling velocity of grains in water. At first glance, there is a clear dependency of settling velocity on grain size (e.g., Alcérreca et al., 2013), although extreme particle densities markedly affect the settling-velocity distribution as well (e.g., Mao et al., 2023). Settling velocities in the dataset range from as slow as 0.003 m s^{-1} to as fast as 0.81 m s^{-1}, with a median of 0.19 m s^{-1} for siliciclastics and 0.074 m s^{-1} for carbonates.

4 Results

4.1 Settling velocity is a function of grain size and shape

The hydrodynamic behaviour of the tested sediment grains in the compilations is expressed by two dimensionless numbers: (i) particle Reynolds number (Re_p, Equation 5), and (ii) experimental drag coefficient, obtained by rewriting Equation 3:

$$C_{D,exp} = \frac{4}{3} D_n \, g \left(\frac{\rho_p}{\rho_f} - 1 \right) \frac{1}{{w_{t,exp}}^2} \tag{6}$$

where $w_{t,exp}$ is the terminal settling velocity observed in experiments. The Re_p – C_D relationships for the experimental results are shown for each compilation individually in Figure 4A. The patchwork appearance of the data reflects the broad spread in grain size, density and shape between datasets. Most data points plot well above the equation for spherical particles, with the rare exception of some of the medium carbonate sand grains of Alcérreca et al. (2013), which reach down to the curve for spheres of Clift & Gauvin (1971). Best-fit second-order polynomial curves are calculated through the data points using the MATLAB curve fitting tool (Figure 4A).

The scattered nature of the data suggests a dependency of the Re_p – C_D relationship on an additional parameter. When the combined data points are grouped by composition and colour-coded by CSF, it becomes apparent that the drag coefficient for a given particle Reynolds number increases with decreasing Corey shape factor (Figure 4B). Therefore, rather than

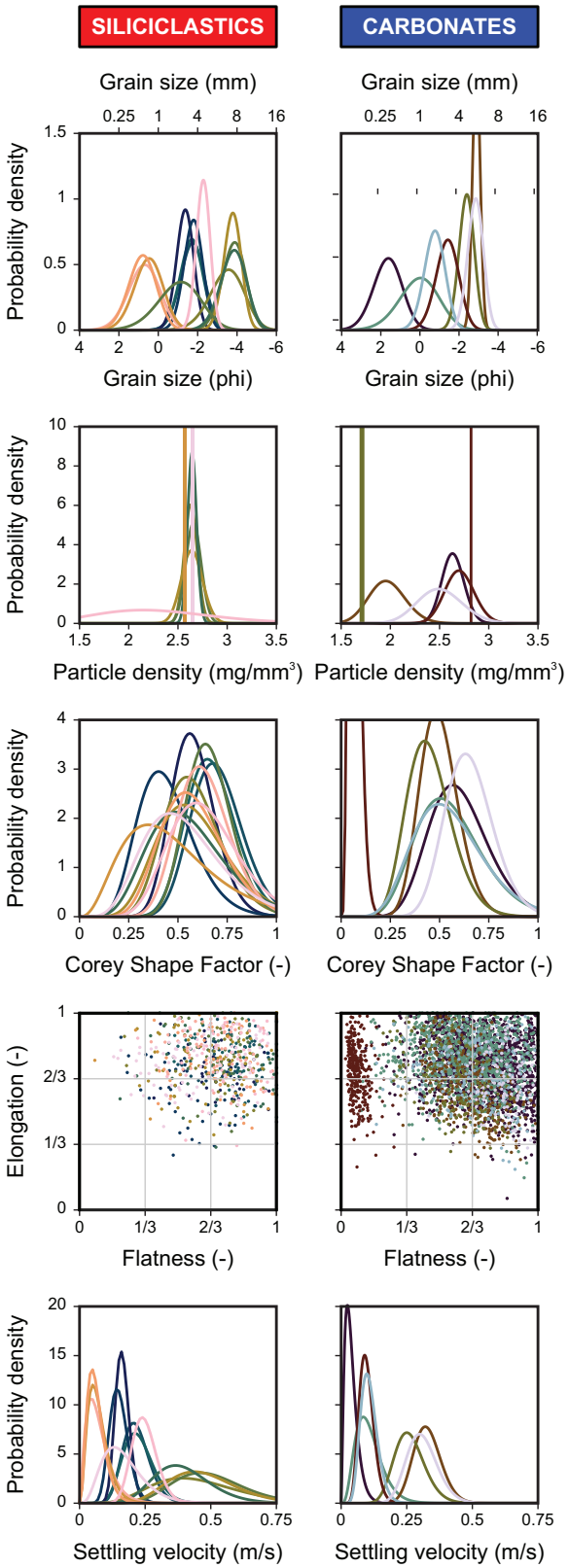

SILICICLASTICS	N = 604	
River sediment		
Corey (1949)	n = 46	qtz, fsp sand
Corey (1949)	n = 48	qtz, fsp sand
Wilde (1952)	n = 44	qtz, fsp gravel
Schulz (1954)	n = 87	qtz, fsp, chd sand
Aeolian sand		
Corey (1949)	n = 37	qtz, fsp sand
Glacial sediment		
Wilde (1952)	n = 36	qtz, fsp gravel
Rock crusher		
Corey (1949)	n = 40	qtz, fsp fragments
Wilde (1952)	n = 35	qtz, fsp fragments
Schulz (1954)	n = 13	fsp fragments
Schulz (1954)	n = 28	qtz fragments
Other		
Wilde (1952)	n = 58	qtz, fsp fragments
Goossens (1987)	n = 92	qtz sand
Riazi & Türker (2019)	n = 40	unspecified

CARBONATES	N = 3 666	
Tropical		
Smith & Cheung (2003)	n = 998	beach sand
Alcérreca et al. (2013)	n = 1 557	beach sand
Wang et al. (2018)	n = 117	reef sediment
Mao et al. (2023)	n = 272	coral debris
Mao et al. (2023)	n = 199	'aquarium' sand
Cool-water		
Slootman et al. (2023)	n = 203	shallow-water (Pleistocene)
Bivalve fragments		
Li et al. (2019)	n = 320	lagoon bivalve fragments

Figure 3 – Particle properties of sediment grains in the siliciclastic and carbonate datasets in the compilations of settling velocity. Both compositions include broad ranges of grain size, density, shape and settling velocity to ensure a wide spread of particle Reynolds numbers. The settling velocity is displayed only for particles falling through water. Abbreviations: qtz = quartz; fsp = feldspar; chd = chalcedony. See Table 1 for details.

a Re_p – C_D curve, the data are likely to define a surface in the Re_p – C_D – CSF parameter space. The coefficients of a second-order polynomial surface are calculated using the MATLAB curve fitting tool (Figure S1 in supplementary materials). The function $C_D = f\left(Re_p, CSF\right)$ is expressed in logarithms with a base of 10 of C_D and Re_p, and is of the form:

$$\begin{aligned}\log_{10}\left(C_D\right) = & p_{00} + \\ & p_{10} \cdot \log_{10}\left(Re_p\right) + \\ & p_{01} \cdot CSF + \\ & p_{11} \cdot \log_{10}\left(Re_p\right) \cdot CSF + \\ & p_{20} \cdot \left[\log_{10}\left(Re_p\right)\right]^2 + \\ & p_{02} \cdot CSF^2\end{aligned} \tag{7}$$

for which the coefficients are as specified in Table 2 (see Equation A2 in Appendix A for non-logarithmic form). The surfaces are plotted in Figure 5. Datapoints are grouped in CSF bins of 0.1 width and plotted on the CSF isoplane on the midpoints. Continuous curves represent the intersection of the surface with the CSF isoplanes. The dashed curves are shown for comparison with the other composition. The grey curves indicate Stokes' Law (stippled) and the Re_p – C_D relationship for spheres (dashed). The function $C_D = f\left(Re_p, CSF\right)$ has a coefficient of determination of $R^2 = 0.7538$ for siliciclastics and $R^2 = 0.8590$ for carbonates.

Table 2 – Coefficients to the second-order polynomial function for $C_D = f(Re_p, CSF)$ in Equation 7.

Siliciclastic	Carbonate
$p_{00} = 1.8045$	$p_{00} = 2.3694$
$p_{10} = -0.6334$	$p_{10} = -0.8715$
$p_{01} = -0.8066$	$p_{01} = -2.7092$
$p_{11} = -0.0758$	$p_{11} = -0.03161$
$p_{20} = 0.09047$	$p_{20} = 0.1237$
$p_{02} = 0.2434$	$p_{02} = 2.1614$

Comparison of the siliciclastic and carbonate curves in Figure 5 reveals that for lower values of the particle Reynolds number ($Re_p \lesssim p$, $p \in [10, 100]$), the predicted drag coefficient for carbonate grains always exceeds that of siliciclastic particles. In contrast, for higher values of the particle Reynolds number ($Re_p \gtrsim p$, $p \in [10, 100]$), at which most sedimentary processes involving sand-sized grains operate, the predicted drag coefficient for siliciclastics is higher than for carbonates for non-spheroidal grains ($CSF < 0.7$). However, for spheroidal grains ($CSF > 0.8$), the drag coefficient for carbonates exceeds that of siliciclastics. The modelled function $C_D = f\left(Re_p, CSF\right)$ tends to fall below Stokes' Law for very low particle Reynolds numbers for siliciclastics. However, due to a lack of data at the lowest particle Reynolds numbers in the siliciclastic compilation, the curves are less reliable in this domain. Predicted drag coefficients for carbonate grains always remain well above Stokes' Law, which, however, may not be realistic either. In other words, the reconstructed surfaces are not reliable for low values of the particle Reynolds number (e.g., $Re_p < 5$). Upper limits of validity of Equation 7 are controlled by the largest particle Reynolds numbers in the compilations. Equation 7 is not valid for Re_p exceeding 10^4 for carbonates and 10^5 for siliciclastics.

4.2 Error in predicted settling velocity

Calculation of the terminal settling velocity $w_{t,calc}$ from $C_D = f\left(Re_p, CSF\right)$ in Equation 7 requires an iteration process, because both Re_p and C_D are functions of w_t. The iteration process (Figure 6) is performed for each grain individually, for which the particle properties as recorded in the experiments are used as input parameters. The first iteration starts with an estimate of the particle Reynolds number (e.g., $Re_p = 100$), which is inserted into Equation 7 to obtain a calculated value of the drag coefficient. The first calculated terminal settling velocity is then computed using Equation 3. A new particle Reynolds number is obtained using this $w_{t,calc}$ through Equation 5. The second iteration starts with using the new particle Reynolds number to calculate a refined drag coefficient, with which a more accurate settling velocity is obtained. The relative error between the first and the second calculated settling velocity is evaluated. If the error is larger than the tolerance of 1 %, then the iteration is repeated until the error falls below the tolerance value. Five iterations were performed here (see Figure S2 in supplementary materials for intermediate steps).

For each grain, the calculated terminal settling velocity obtained from the final iteration is compared with the terminal settling velocity observed in experiment by calculating the relative error:

$$\varepsilon = \left(\frac{w_{t,calc}}{w_{t,exp}} - 1\right) \cdot 100\,\% \tag{8}$$

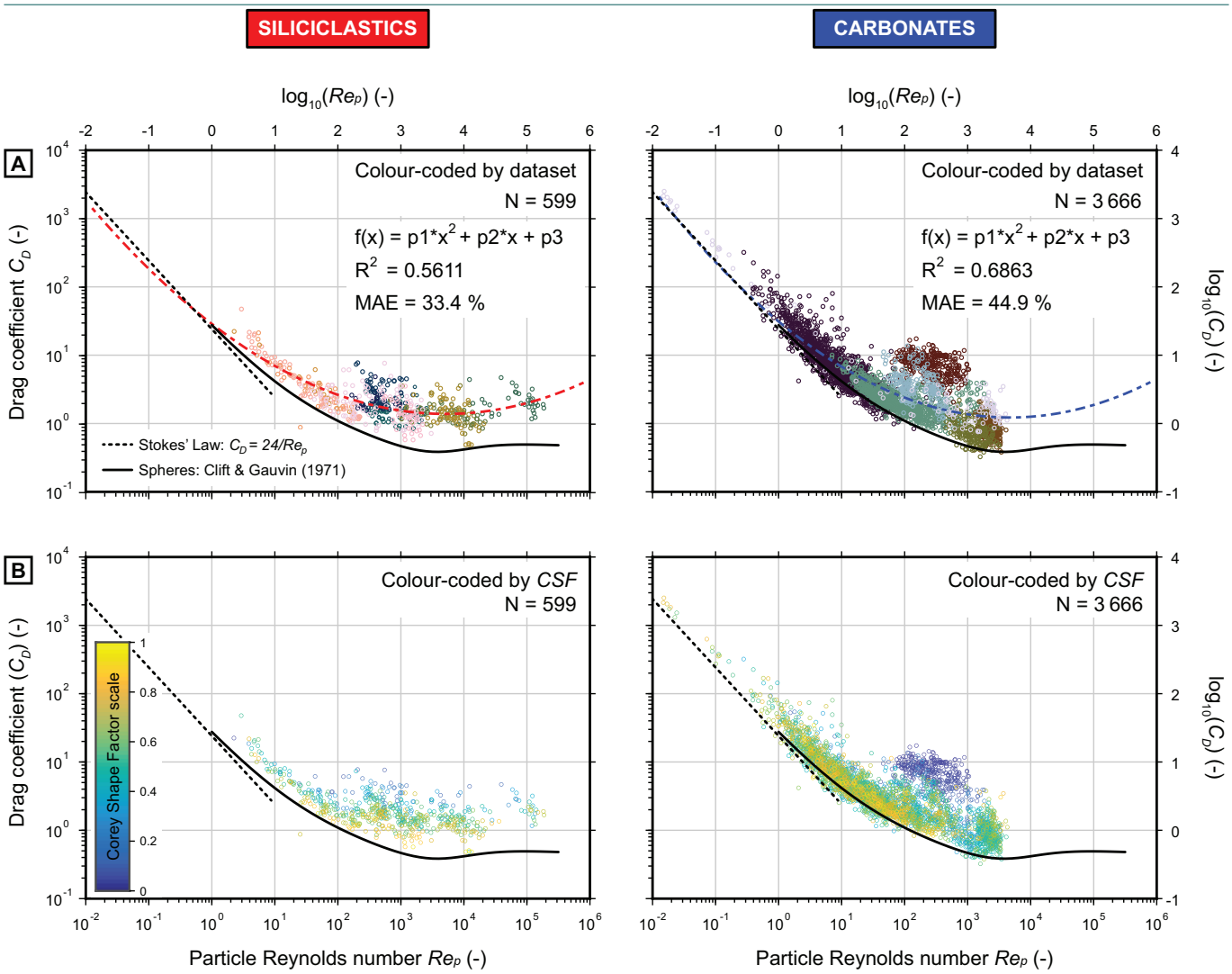

Figure 4 – Hydrodynamics of siliciclastic and carbonate sediment grains in the parameter space of particle Reynolds number and drag coefficient. **(A)** Displayed by dataset. The red and blue dashed curves display the best-fit second-order polynomial function $f(x)$, where $f(x)$ represents C_D and x represents Re_p. The coefficients for siliciclastics are $p1 = 0.0957$, $p2 = -0.7103$, and $p3 = 1.4580$. The coefficients for carbonates are $p1 = 0.1042$, $p2 = -0.7652$, and $p3 = 1.4928$. Datasets are coloured as in Figure 3. **(B)** Displayed by Corey shape factor. As *CSF* decreases, C_D for a given Re_p increases. Stokes' Law and the curve for spheres (Clift & Gauvin, 1971) are shown for reference.

The results of the final iteration and the corresponding error distribution for the siliciclastic and carbonate compilations are shown in Figure 7. The mean absolute error *MAE* indicates the degree of scatter of the data from the 1:1 relationship, on which the calculated settling velocities exactly match the experimental settling velocities:

$$MAE = \frac{1}{n}\sum abs(\varepsilon) \quad (9)$$

Error analysis helps evaluating the performance of the function $C_D = f(Re_p, CSF)$ in Equation 7 for the prediction of particle settling velocity. Since the function utilizes the nominal diameter and Corey shape factor, the error analysis provides insights into the validity of these parameters as grain descriptors in the ellipsoidal particle model.

The data points in the carbonate compilation display a higher degree of scatter than in the siliciclastic compilation (Figure 7). The majority of observed versus predicted settling velocities plot within the 25 % error envelope. For siliciclastics, 82 % plots within the error envelope, 12 % above, and 6 % below. For carbonates, more data points than for siliciclastics plot outside the envelope: 66 % plots within, 19 % above, and 15 % below. Also when analysed individually, siliciclastic datasets maintain narrower error distributions than carbonate datasets (see Figures S3 and S4 in supplementary materials). The higher degree of scatter for carbonates is reflected by the larger mean absolute error in comparison to

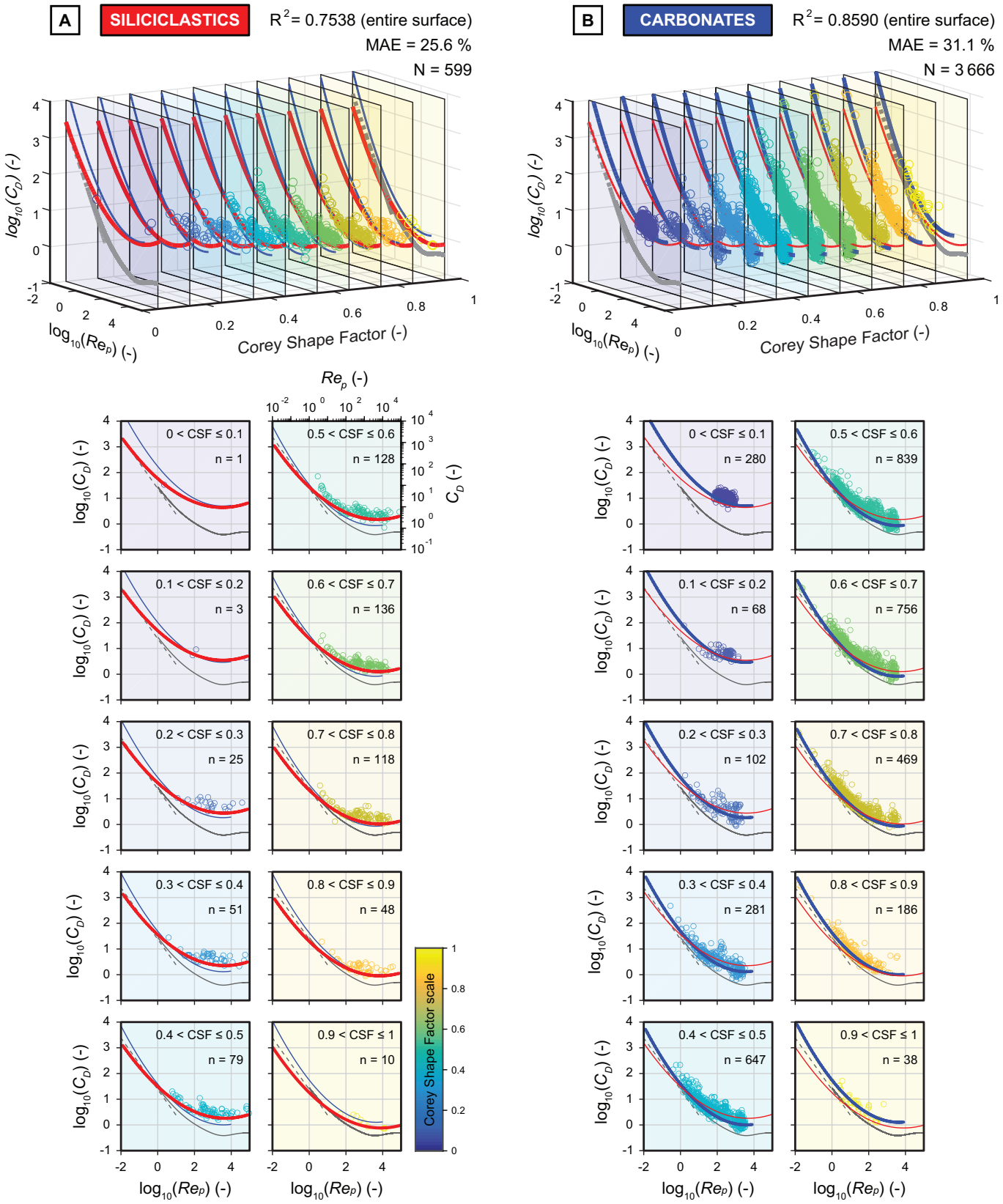

Figure 5 – The relationship $C_D = f(Re_p, CSF)$ for the compilations of **(A)** siliciclastic and **(B)** carbonate grains. The surface is the second-order polynomial function in Equation 7 for particle Reynolds number and drag coefficient expressed as logarithms with a base of 10, with the coefficients in Table 2. Data points are grouped in *CSF* bins. Red and blue curves represent the intersection between the polynomial surface and the *CSF* isoplanes for siliciclastics and carbonates, respectively. Stokes' Law and the curve for spheres (Clift & Gauvin, 1971) are shown for reference.

the *MAE* of siliciclastics. (Although, mean absolute errors improved from using the equations for drag coefficient that do not depend on Corey shape factor to the *CSF*-dependent equations, from 33 % to 14 % for siliciclastics and from 45 % to 21 % for carbonates.)

The mean μ of the error distribution measures the accuracy of the predictive settling velocity model, whereas the precision of the model is indicated by the standard deviation σ. For siliciclastics, the combination of the low mean (μ_{SiO_2} = 1.7 %) and the approximately symmetrical distribution of the error around the mean, demonstrate that the predicted settling velocities for siliciclastic particles have a relatively high accuracy and are not skewed towards higher or lower values, but are symmetrically scattered around the 1:1 relationship for observed versus predicted velocities. The carbonate model has a comparable, yet slightly lower, accuracy as indicated by the mean (μ_{CaCO_3} = 4.4 %). However, the precision of the model is much lower for carbonates (σ_{CaCO_3} = 32 %) than for siliciclastics (σ_{SiO_2} = 19 %), in line with the higher degree of scatter in the experimental versus calculated settling velocities in the carbonate compilation. In addition, the error distribution of the carbonate model is positively skewed towards higher values. This asymmetry implies that the carbonate compilation contains more particles for which the settling velocity has been overestimated than in the siliciclastic compilation. This is due to genetic differences between carbonate and siliciclastic sediment grains, as further explored in the next section.

5 Discussion

5.1 Differences between carbonate and siliciclastic sediments

In the carbonate compilation, the relative error between predicted and measured settling velocity is skewed towards positive values (Figure 7). A positive error implies that the calculated settling velocity exceeds the measured velocity. This difference results from the predicted influence of gravity being over-represented, and/or the under-representation of fluid drag on the particle in the ellipsoidal model. Predicted settling velocities exceeding measured values may be caused by one or more of the following: (i) the actual grain volume is smaller than that of the ellipsoid for which the settling velocity was calculated, (ii) the particle has lower density than modelled, (iii) the grain experiences more friction than expected from the elliptical maximum projection area in the ellipsoidal particle model, (iv) there is more resistance caused by fluid passing sharp particle corners, (v) rough grain surfaces cause additional drag that is not accounted for in the ellipsoidal particle model. Negative errors also occur, in almost equal proportion, yet with less extreme values. Both positive and negative errors also emerge in the siliciclastic compilation, however siliciclastics errors are smaller and the error distribution is symmetrical instead. This suggests that the ellipsoidal model is better suitable for the description of siliciclastic particles than for carbonate grains, most likely due to irregularities in first-order shape (i.e., form as described by ellipsoidity), as well as second-order (i.e., angularity or roundness) and third-order (i.e., surface texture) shape properties (see Barrett, 1980; Griffiths, 1967; as reviewed in De Kruijf et al., 2021). In addition, asymmetries in the distribution of shape and/or density may exist for individual grains, which are unaccounted for in the ellipsoidal particle model.

5.2 Particle shape dependency in other studies

The number of studies that investigated the effect of shape quantified as ellipsoidity using Corey shape factor on the hydrodynamic behaviour of natural sediments is limited. Notable exceptions include Alger (1964), who settled a couple dozen siliciclastic gravel-sized clasts supplemented with regular geometric shapes, and Smith & Cheung (2003), who tested the settling of nearly one thousand tropical carbonate sand grains. These studies reconstructed curves for the drag coefficient as a function of particle Reynolds number for several values of the Corey shape factor based on original data. Only two other studies, utilizing previously published datasets, proposed C_D – Re_p relationships as a function of *CSF* (Swamee & Ojha, 1991; Wu & Wang, 2006). The curves of these four studies are shown in Figure 8, together with the curves representing the intersection between the Corey shape factor isoplanes and the surfaces found in this study.

All six sets of curves in Figure 8 indicate decreasing drag coefficients for increasing particle Reynolds numbers in the laminar regime (Re_p < 10). Fully turbulent conditions are only reached for particle Reynolds numbers exceeding $Re_p = 10^5$ (see Figure 2), which are achieved by none of the particles in the compilations. By far, the bulk of the analysed

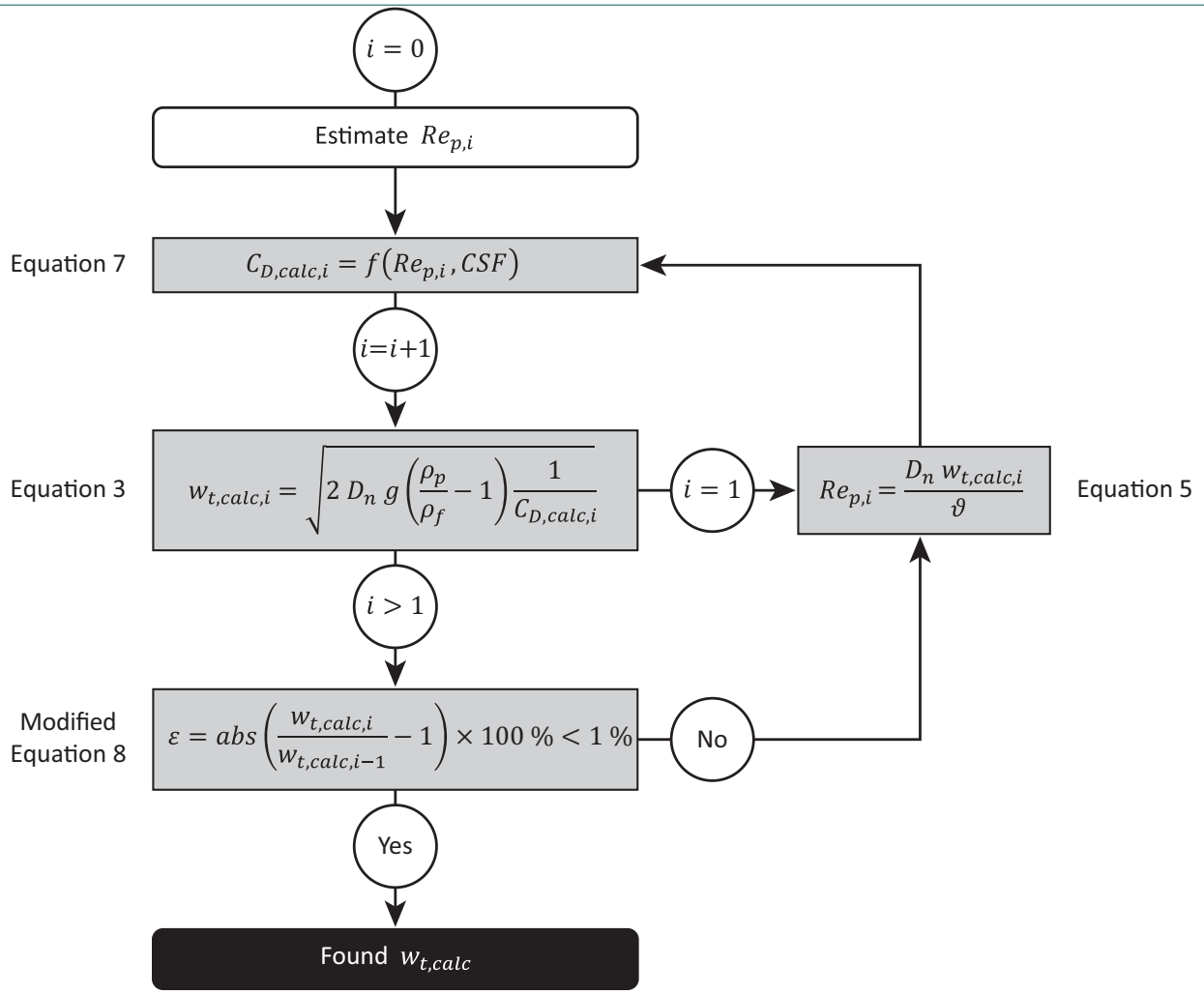

Figure 6 – Iteration process for the calculation of terminal settling velocity using particle and fluid properties for the *i*-th iteration. See subsection 4.2 for details.

grains settled in the transitional regime (96 % for siliciclastics, 77 % for carbonates). Hydrodynamics in the transitional regime is complicated and has not been resolved theoretically, hence requiring empirical solutions (Allen, 1982; Dey et al., 2019). However, the general C_D – Re_p dependency consistently demonstrates that with particle Reynolds numbers increasing beyond the laminar regime and into the transitional regime, the drag coefficient drops further until a minimum value is reached (Dey et al., 2019). From this 'trough' in the curve, C_D again rises for higher Re_p but with a lower rate on double-logarithmic scale (Figure 2). All curves in Figure 8, including the solution for spheres of Clift & Gauvin (1971), display the characteristic trough of the transitional regime. The equation for spheres halts at a plateau with constant drag coefficient, a trend mimicked by the siliciclastic curves of Alger (1964) and Swamee & Ojha (1991), and to some extent by the curves of Wu & Wang (2006). The curves for carbonates of Smith & Cheung (2003) display strong curvature due to the rapid increase in C_D towards higher Re_p beyond the trough. However, the curves of Smith & Cheung (2003), for which no goodness of fit is reported, are data-limited to support the continuation of the strong curvature towards higher particle Reynolds numbers.

Smith & Cheung (2003) remark that for lower *CSF* values, the onset of the transitional regime shifts towards lower Re_p. This trend is persistent in all studies, including the present compilations, as demonstrated by the migrating position of the troughs in the curves. The constant drag coefficients reached for the siliciclastic curves at the higher end of Re_p, are not apparent in the siliciclastic surface reconstructed in this study. Potentially, this is a result of the choice for a second-order polynomial function for the C_D – Re_p – *CSF* surface, which never reaches a plateau. Yet, the reconstructed surfaces attain good fits within the domain of particle Reynolds numbers in the compilations (i.e., $Re_p \lesssim q$, $q \in [10^4, 10^5]$). Although

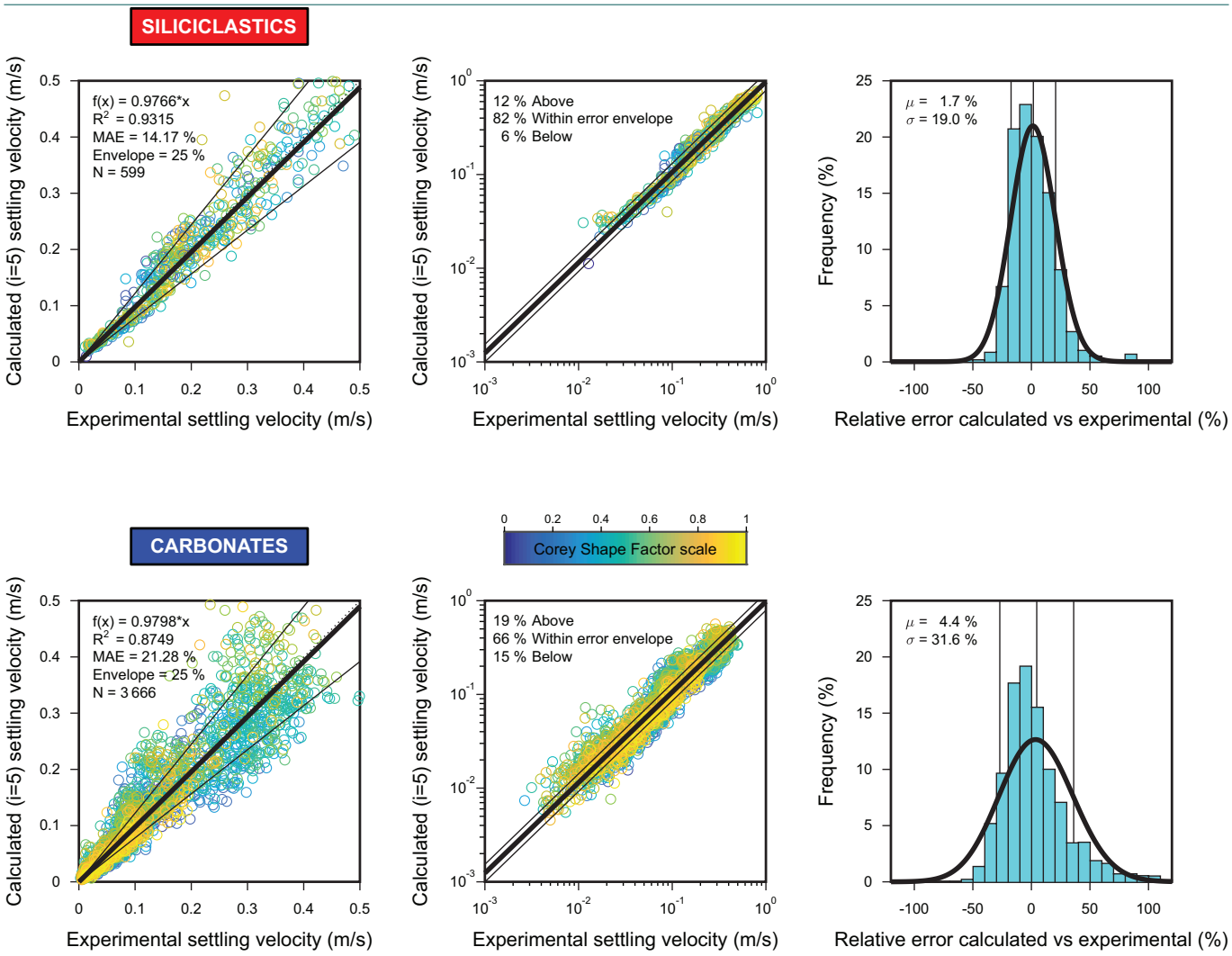

Figure 7 – Observed versus predicted settling velocity (fifth iteration) on linear and logarithmic scales. The function $f(x)$ is the best fit of linear regression passing through the origin with coefficient R^2. Mean absolute error (*MAE*, Equation 9) and the 25 % error envelope are shown. Relative error is calculated using Equation 8. Histograms and corresponding normal gamma probability density functions show the distribution of relative error. The mean μ and standard deviation σ of the distribution are indicated, which respectively provide a measure of accuracy and precision of the settling velocity model.

the previously proposed curves are in accordance with the trends of the surfaces found in this study, all these curves plot at lower drag coefficients, i.e., below the reconstructed surfaces.

There is a striking difference between the siliciclastic and carbonate surfaces reconstructed in this study. For a given particle Reynolds number on the siliciclastic surface, the drag coefficient always increases as grains become more ellipsoidal with decreasing *CSF*. For the reconstructed carbonate surface, this trend is valid only for Corey shape factors smaller than $CSF = 0.6$. Instead, the drag coefficient for carbonates with a given Re_p increases as grains become more spheroidal as Corey shape factors increase from $CSF = 0.7$ onwards. This odd trend in the reconstructed hydrodynamic behaviour of carbonate grains is explained by the irregularity of skeletal particles.

5.3 Influence of carbonate grain irregularity

The distribution of the error in calculated versus measured settling velocity is not a function of Corey shape factor, nor of particle size as represented by particle Reynolds number or nominal diameter (see Figures S5 and S6 in supplementary materials). This implies that the $C_D - Re_p$ relationships reconstructed in this study (Figure 8A, E) are indeed representative of the hydrodynamic behaviour of the grains in the siliciclastic and carbonate compilations. A dependency of these curves on the Corey shape factor was found. For siliciclastics, the calculated curves predict that the drag coefficient for a given particle Reynolds number decreases as *CSF* increases. In other words, less spheroidal shapes (i.e., flatter or more elongated

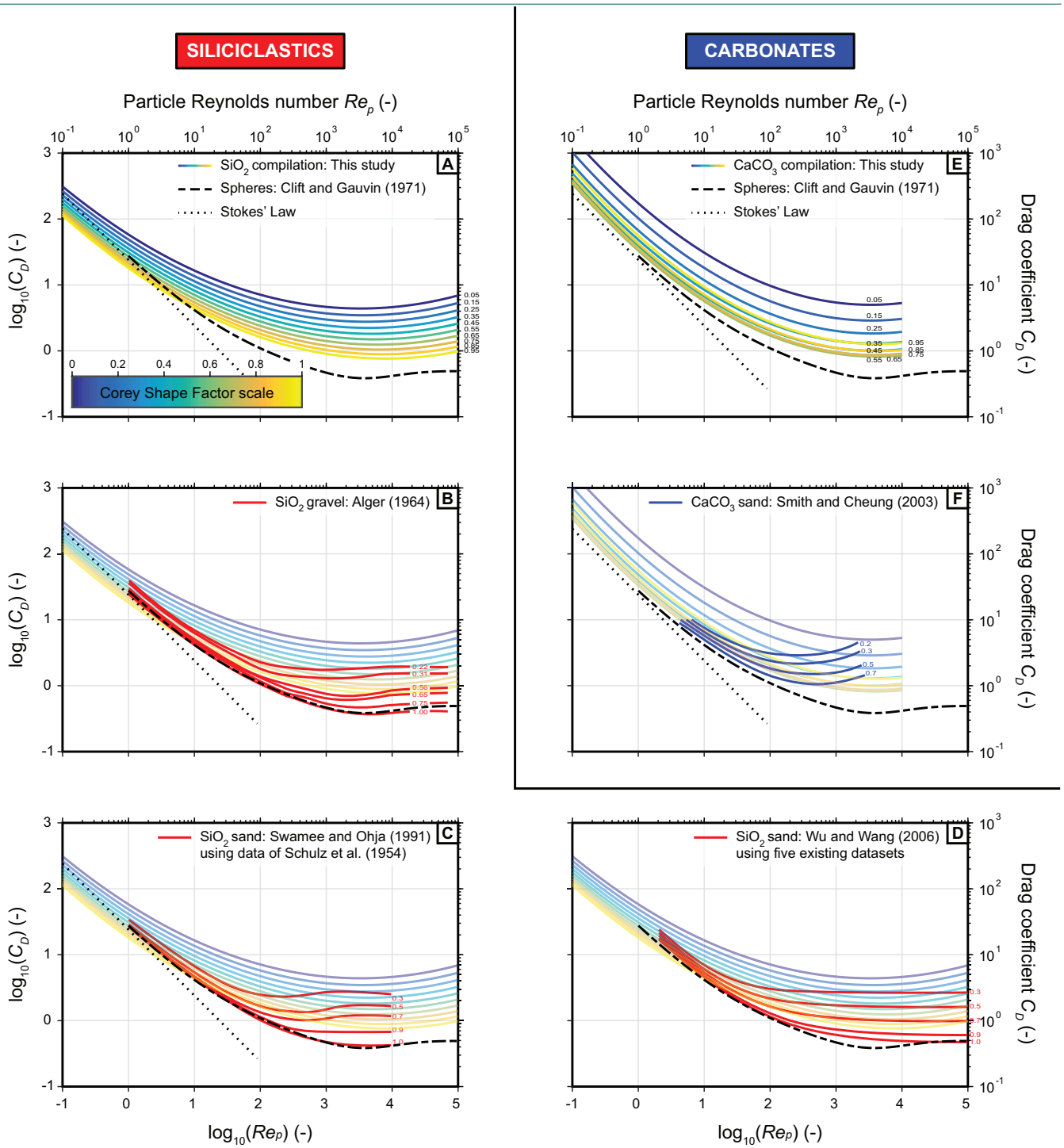

Figure 8 – Trendlines for the Re_p – C_D relationship as a function of Corey shape factor. Colour-coded curves represent the intersections between the calculated surfaces and *CSF*-isoplanes as shown in Figure 5. Corey shape factor dependencies found in other studies are displayed for **(A–D)** siliciclastic (red) and **(E–F)** carbonate grains (blue). Numbers correspond to *CSF* values. Wu & Wang (2006) used the datasets of Corey (1949), Krumbein (1941), Romanovskii (1972), Schulz et al. (1954) and Wilde (1952).

grains) experience more drag than spheroidal ones. However, the curve for the most-spheroidal grains does not reach down to the solution for spheres of Clift & Gauvin (1971), demonstrating that these particles experience more drag than predicted for perfect spheres. Also for carbonate grains the drag coefficient for a given particle Reynolds number decreases as grains become more spheroidal with increasing *CSF*, however, only up to a value of *CSF* = 0.6. For more-spheroidal grains with larger Corey shape factors, the drag coefficient for a given Re_p increases with about 50 % for Corey shape factors up to *CSF* = 1. This peculiar observation confirms that for more-spheroidal grains, ellipsoidity does not

sufficiently predict grain size and shape. For example, higher-order shape factors (i.e., angularity and surface roughness) may become more important as Corey shape factor increases, or particle asymmetry starts playing a more significant role for less-elongated and less-flat grains.

The conclusion that the ellipsoidal model alone is not sufficient to describe grain shape is not new. The widely accepted equations for settling velocity of Dietrich (1982) account for grain shape by applying both the Corey shape factor and Powers (1953) roundness, which is a semi-quantitative visual chart, to account for the influence of second- and third-order shape properties (see De Kruijf et al., 2021 for a discussion and review). Due to the impracticability of determining this combination of shape descriptors, Dietrich (1982) proposed values appropriate for "natural sediment particles", as later repeated by Ferguson & Church (2004). However, there are no quantitative data available to evaluate such standard values, yet these values are commonly used in literature and engineering applications. Goossens (1987b) performed theoretical sensitivity analyses to validate the use of Dietrich's (1982) combination of shape parameters, finding that for small particles the influence of grain angularity on settling velocity decreases as spheroidicity increases. Strikingly, the opposite holds true for larger particles, for which settling velocity is increasingly more influenced by grain angularity as particles become more spheroidal (Goossens, 1987b). The implications of these discoveries for the curves reconstructed for the carbonate compilation in Figure 8E are that in the domain of higher particle Reynolds numbers, the increasing drag coefficients for more-spheroidal grains may be explained by the high degree of irregularity of the carbonate grains. The influence of grain irregularity and surface roughness on the $C_D - Re_p$ relationships for larger values of the Corey shape factor ($CSF \geq 0.7$) is perhaps such that curves are 'pulled up' towards higher values of the drag coefficient.

6 Conclusions on the validity of the ellipsoidal particle model

This paper set out to test the validity of the ellipsoidal particle model in settling velocity problems. Parameters tied to the ellipsoidal model are the nominal diameter for grain size, and the Corey shape factor for grain shape. The suitability of these particle descriptors was evaluated for large compilations of siliciclastic and carbonate sediments. Equations were established for the drag coefficient (representing friction) as a function of particle Reynolds number (representing particle size in the range $5 < Re_p \lesssim q$, $q \in [10^4, 10^5]$) and Corey shape factor (representing ellipsoidity). With these equations, settling velocities were predicted using reported particle and fluid properties, which were then compared with the velocities measured in experiments. Mean absolute errors of predicted drag coefficients are significantly reduced when Corey shape factor is considered. This is reflected by smaller errors in predicted settling velocity; from 33 % to 14 % for siliciclastic particles and from 45 % to 21 % for carbonate grains. Although reduced, these errors imply that the ellipsoidal particle descriptors, i.e., nominal diameter and Corey shape factor, do not fully capture the size and shape of natural sediments. In particular, the modelling of irregular grains such as carbonates as ellipsoids is problematic. Yet, this is common practice in both sedimentology and engineering, perhaps based on the simplistic assumption that tri-axial ellipsoids offer an appropriate representation of carbonate particles. Alternative grain-size and shape descriptors exist, in particular the simple volume/area ratio of grains, as further explored in the companion paper to this publication (*Part 2*, Slootman et al., 2026).

Acknowledgements

Dr. Alcérreca, Dr. Wang, and Prof. Cheung are thanked for sharing the unpublished data used in their publications. We are indebted to Dr. Urs Neumeier, Yuhao Li, and an anonymous reviewer for their insightful comments that helped improve the quality of our work. Associate Editor Dr. Siddhi Joshi and Executive Editor Prof. Murray Gingras are acknowledged for their efforts in coordinating the review process. We thank Dr. Jarred Lloyd, production manager of Sedimentologika, for his assistance in refining the presentation of our paper.

Data and code availability

A table with all data in the format of a spreadsheet, and the MATLAB script used to plot the figures are uploaded as supplementary materials.

Supplementary materials

Supplementary material to this article can be found online at: doi:10.57035/journals/sdk.2026.e41.1937

Conflict of interest statement

The authors declare they do not have any tangible or perceived conflicts of interest with regard to this research.

Artificial intelligence use statement

All research, analysis, writing, and editing were performed without generative AI assistance.

Funding

The authors received no specific funding for this work.

Citing this Research Article

To cite this paper use the following information:

Authors
Arnoud Slootman, Max de Kruijf, Guenther Glatz, Joris T. Eggenhuisen, Zane R. Jobe, John J. G. Reijmer

Title
Settling velocity of sediment grains, Part 1: Natural sediment particles are not ellipsoids

Short Title
Settling velocity: Natural sediment particles are not ellipsoids

Publishing Information
Publication: Sedimentologika
Volume: 4
Issue: 1
Year: 2026
DOI: 10.57035/journals/sdk.2026.e41.1937
Language: en

Appendix A

Table A1 – Symbols and descriptions of parameters used in in equations, figures and tables in this article in this article.

Symbol	Description
A	Particle maximum projection area
$abs(\varepsilon)$	Absolute error
C_D	Drag coefficient
$C_{D,exp}$	Experimental drag coefficient
CSF	Corey shape factor
D_{eq}	Equivalent particle diameter
D_i	Intermediate particle diameter
D_l	Long particle diameter
D_n	Nominal particle diameter
D_s	Short particle diameter
F_D	Drag force
F'_g	Submerged weight
g	Gravitational acceleration
i	Index counting iterations
MAE	Mean absolute error
n	Number of measurements
N	Number of datasets
p_{00}	Coefficient to the polynomial function in Equation 7
p_{10}	Coefficient to the polynomial function in Equation 7
p_{01}	Coefficient to the polynomial function in Equation 7
p_{11}	Coefficient to the polynomial function in Equation 7
p_{20}	Coefficient to the polynomial function in Equation 7
p_{02}	Coefficient to the polynomial function in Equation 7
Re_p	Particle Reynolds number
V	Particle volume
w	Settling velocity
w_t	Terminal settling velocity
$w_{t,calc}$	Calculated terminal settling velocity
$w_{t,exp}$	Experimental terminal settling velocity (observed)
ε	Relative error
μ	Mean (model accuracy)
μ	Dynamic fluid viscosity
ϑ	Kinematic fluid viscosity
ρ_f	Fluid density
ρ_p	Particle density
σ	Standard deviation (model precision)

Relationship for spherical particles between drag coefficient and particle Reynolds number by Clift & Gauvin (1971), which is valid for $Re_p < 3 \times 10^5$:

$$C_D = \frac{24}{Re_p\left(1 + 0.15{Re_p}^{0.687}\right)} + \frac{0.42}{\left(1 + \frac{42\,500}{{Re_p}^{1.16}}\right)} \quad \text{(A1)}$$

Rewritten form of Equation 7:

$$C_D = 10\text{^}\left(p_{00} + p_{10} \times \lg\left(Re_p\right) + p_{01} \times CSF + p_{11} \times \lg\left(Re_p\right) \times CSF + p_{20} \times \left[\lg\left(Re_p\right)\right]^2 + p_{02} \times CSF^2\right) \quad \text{(A2)}$$

References

Alcérreca, J. C., Silva, R., & Mendoza, E. (2013). Simple settling velocity formula for calcareous sand. *Journal of Hydraulic Research*, *51*(2), 215–219. https://doi.org/10.1080/00221686.2012.753645

Alger, G. R. (1964). *Terminal fall velocity of particles of irregular shapes as affected by surface area* [Doctoral dissertation, Colorado State University]. https://doi.org/10.25675/3.025083

Allen, J. R. L. (Ed.). (1982). *Sedimentary Structures—Their Character and Physical Basis Volume I: Vol. Developments in Sedimentology: 30A*. Elsevier.

Allen, J. R. L. (1984). Experiments on the settling, overturning and entrainment of bivalve shells and related models. *Sedimentology*, *31*(2), 227–250. https://doi.org/10.1111/j.1365-3091.1984.tb01961.x

Baba, J., & Komar, P. D. (1981). Settling Velocities of Irregular Grains at Low Reynolds Numbers. *Journal of Sedimentary Research*, *51*(1), 121–128. https://doi.org/10.1306/212f7c25-2b24-11d7-8648000102c1865d

Bagheri, G. H., & Bonadonna, C. (2016). On the drag of freely falling non-spherical particles. *Powder Technology*, *301*, 526–544. https://doi.org/10.1016/j.powtec.2016.06.015

Barrett, P. J. (1980). The shape of rock particle, a critical review. *Sedimentology*, *27*, 291–303. https://doi.org/10.1111/j.1365-3091.1980.tb01179.x

Blott, S. J., & Pye, K. (2008). Particle shape: A review and new methods of characterization and classification. *Sedimentology*, *55*(1), 31–63. https://doi.org/10.1111/j.1365-3091.2007.00892.x

Braithwaite, C. J. R. (1973). Settling behaviour related to sieve analysis of skeletal sands. *Sedimentology*, *20*(2), 251–262. https://doi.org/10.1111/j.1365-3091.1973.tb02048.x

Briggs, L. I., McCulloch, D. S., & Moser, F. (1962). The hydraulic shape of sand particles. *Journal of Sedimentary Research*, *32*(4), 645–656. https://doi.org/10.1306/74D70D44-2B21-11D7-8648000102C1865D

Camenen, B., Bayram, A., & Larson, M. (2006). Equivalent Roughness Height for Plane Bed under Steady Flow. *Journal of Hydraulic Engineering*, *132*(11), 1146–1158. https://doi.org/10.1061/(ASCE)0733-9429(2006)132:11(1146)

Caromel, A. G. M., Schmidt, D. N., Phillips, J. C., & Rayfield, E. J. (2014). Hydrodynamic constraints on the evolution and ecology of planktic foraminifera. *Marine Micropaleontology*, *106*, 69–78. https://doi.org/10.1016/j.marmicro.2014.01.002

Cassel, M., Lavé, J., Recking, A., Malavoi, J. R., & Piégay, H. (2021). Bedload transport in rivers, size matters but so does shape. *Scientific Reports*, *11*(1), 1–11. https://doi.org/10.1038/s41598-020-79930-7

Cheng, K. Y., Wang, P. K., & Wang, C. K. (2014). A numerical study on the ventilation coefficients of falling hailstones. *Journal of the Atmospheric Sciences*, *71*(7), 2625–2634. https://doi.org/10.1175/JAS-D-13-0229.1

Clift, R., & Gauvin, W. H. (1971). Motion of entrained particles in gas streams. *Canadian Journal of Chemical Engineering*, *49*(4), 439–448. https://doi.org/10.1002/cjce.5450490403

Clift, R., Grace, J. R., & Weber, M. E. (1978). *Bubbles, drops, and particles*. Academic Press.

Collins, M. B., & Rigler, J. K. (1982). The use of settling velocity in defining the initiation of motion of heavy mineral grains, under unidirectional flow. *Sedimentology*, *29*(3), 419–426. https://doi.org/10.1111/j.1365-3091.1982.tb01804.x

Corey, A. T. (1949). *Influence of shape on the fall velocity of sand grains* [Master thesis, Colorado Agricultural and Mechanical College]. https://doi.org/10.25675/3.025499

De Kruijf, M., Slootman, A., De Boer, R. A., & Reijmer, J. J. G. (2021). On the settling of marine carbonate grains: Review and challenges. *Earth-Science Reviews*, *January*, 103532–103532. https://doi.org/10.1016/j.earscirev.2021.103532

Dey, S., & Ali, S. Z. (2019). Bed sediment entrainment by streamflow: State of the science. *Sedimentology*, *66*(5), 1449–1485. https://doi.org/10.1111/sed.12566

Dey, S., Ali, S. Z., & Padhi, E. (2019). Terminal fall velocity: the legacy of Stokes from the perspective of fluvial hydraulics. *Proceedings of the Royal Society A: Mathematical, Physical and Engineering Sciences*, *475*(2228), 20190277. https://doi.org/10.1098/rspa.2019.0277

Dietrich, W. E. (1982). Settling velocity of natural particles. *Water Resources Research*, *18*(6), 1615–1626. https://doi.org/10.1029/WR018i006p01615

Egiazaroff, I. V. (1965). Calculation of Nonuniform Sediment Concentrations. *Journal of the Hydraulics Division*, *91*(4), 225–247. https://doi.org/10.1061/JYCEAJ.0001277

Fan, M., Su, D., & Yang, L. (2022). Development of a benchmark for drag correlations of nonspherical particles based on settling experiments of super-ellipsoidal particles. *Powder Technology*, *409*. https://doi.org/10.1016/j.powtec.2022.117811

Ferguson, R. I., & Church, M. (2004). A simple universal equasion for grain settling velosity. *Journal of Sedimentary Research*, *74*(6), 933–937. https://doi.org/10.1306/051204740933

Fornberg, B. (1988). Steady viscous flow past a sphere at high Reynolds numbers. *Journal of Fluid Mechanics*, *190*, 471–489. https://doi.org/10.1017/S0022112088001417

Francalanci, S., Paris, E., & Solari, L. (2021). On the prediction of settling velocity for plastic particles of different shapes. *Environmental Pollution*, *290*(August), 118068–118068. https://doi.org/10.1016/j.envpol.2021.118068

Ganti, V., Lamb, M. P., & McElroy, B. (2014). Quantitative bounds on morphodynamics and implications for reading the sedimentary record. *Nature Communications*, *5*, 1–7. https://doi.org/10.1038/ncomms4298

Ghoddousi, P., Shirzadi Javid, A. A., & Sobhani, J. (2014). Effects of particle packing density on the stability and rheology of self-consolidating concrete containing mineral admixtures. *Construction and Building Materials*, *53*, 102–109. https://doi.org/10.1016/j.conbuildmat.2013.11.076

Goossens, D. (1987a). A drag coefficient equation for natural, irregularly shaped particles. *Catena*, *14*(1–3), 73–99. https://doi.org/10.1016/S0341-8162(87)80007-3

Goossens, D. (1987b). Interference phenomena between particle flattening and particle rounding in free vertical sedimentation processes. *Sedimentology*, *34*(1), 155–167. https://doi.org/10.1111/j.1365-3091.1987.tb00567.x

Griffiths, J. C. (1967). *Scientific Method in Analysis of Sediments*. McGraw-Hill.

Hjulström, F. (1935). Studies in the morphological activity of rivers as illustrated by the river Fyris. *Bulletin Geological Institute Uppsala*, *XXV*, 221–527.

Joshi, S., Duffy, G. P., & Brown, C. (2014). Settling velocity and grain shape of maërl biogenic gravel. *Journal of Sedimentary Research*, *84*(8), 718–727. https://doi.org/10.2110/jsr.2014.51

Komar, P. D. (1980). Settling velocities of circular cylinders at low Reynolds numbers. *Journal of Geology*, *88*(3), 327–336. https://doi.org/10.1086/628510

Komar, P. D., & Reimers, C. E. (1978). Grain Shape Effects on Settling Rates. *Journal of Geology*, *86*(2), 193–209. https://doi.org/10.1086/649674

Krumbein, W. C. (1938). Size Frequency Distributions of Sediments and the Normal Phi Curve. *Journal of Sedimentary Research*, *8*. https://doi.org/10.1306/D4269008-2B26-11D7-8648000102C1865D

Krumbein, W. C. (1941). The Effects of Abrasion on the Size, Shape and Roundness of Rock Fragments. *Journal of Geology*, *49*(5), 482–520. https://doi.org/10.1086/624985

Lamb, M. P., McElroy, B., Kopriva, B., Shaw, J., & Mohrig, D. (2010). Linking river-flood dynamics to hyperpycnal-plume deposits: Experiments, theory, and geological implications. *Bulletin of the Geological Society of America*, *122*(9–10), 1389–1400. https://doi.org/10.1130/B30125.1

Le Roux, J. P. (2005). Grains in motion: A review. *Sedimentary Geology*, *178*(3–4), 285–313. https://doi.org/10.1016/j.sedgeo.2005.05.009

Li, Y., Yu, Q., Gao, S., & Flemming, B. W. (2020). Settling velocity and drag coefficient of platy shell fragments. *Sedimentology*, *67*(4), 2095–2110. https://doi.org/10.1111/sed.12696

Maiklem, W. R. (1968). Some Hydraulic Properties of Bioclastic Carbonate Grains. *Sedimentology*, *10*(2), 101–109. https://doi.org/10.1111/j.1365-3091.1968.tb01102.x

Mao, L., Li, J., Shimozono, T., & Tajima, Y. (2023). Impacts of Particle Shape, Skeletal Porosity and Density on the Settling Velocity of Gravel-Size Coral Debris. *Journal of Geophysical Research: Earth Surface*, *128*(5), e2022JF006996. https://doi.org/10.1029/2022JF006996

Martin, D., & Nokes, R. (1988). Crystal settling in a vigorously convecting magma chamber. *Nature*, *332*(7), 534–536. https://doi.org/10.1038/332534a0

McKay, G., Murphy, W. R., & Jodieri-Dabbaghzadeh, S. (1989). Settling and Fluidisation Characteristics of Carrot Particles in Water. *Irish Journal of Food Science and Technology*, *13*(1), 51–69. https://www.jstor.org/stable/25580941

Middleton, G. V., & Southard, J. B. (Eds.). (1984). *Mechanics of Sediment Movement: Vol. SEPM Short Course Notes: 3*. SEPM Society for Sedimentary Geology. https://doi.org/10.2110/scn.84.03

Miedema, S. A. (2010). Constructing the shields curve, a new theoretical approach and its applications. In J. Dobson (Ed.), *Proceedings of the 19th world dredging congress* (pp. 732–750). Chida. https://www.researchgate.net/publication/228750218

Mulder, T., & Alexander, J. (2001). The physical character of subaqueous sedimentary density flows and their deposits. *Sedimentology*, *48*(2), 269–299. https://doi.org/10.1046/j.1365-3091.2001.00360.x

Musso, M. S., Slootman, A., Wood, L. J., & Jobe, Z. R. (2025). Stalked crinoids: From skeleton to sediment. *Journal of Sedimentary Research*, *95*(6), 1056–1062. https://doi.org/10.2110/jsr.2025.099

Olivera, A. M., & Wood, W. L. (1997). Hydrodynamics of bivalve shell entrainment and transport. *Journal of Sedimentary Research*, *67*(3), 514–526. https://doi.org/10.1306/D42685B8-2B26-11D7-8648000102C1865D

Polorigni, C. L., Ikumi, D. S., & Ekama, G. A. (2021). Primary sedimentation modelling with characterized setting velocity groups. *Water Research*, *189*, 116621. https://doi.org/10.1016/j.watres.2020.116621

Poulidis, A. P., Biass, S., Bagheri, G., Takemi, T., & Iguchi, M. (2021). Atmospheric vertical velocity - a crucial component in understanding proximal deposition of volcanic ash. *Earth and Planetary Science Letters*, *566*. https://doi.org/10.1016/j.epsl.2021.116980

Powers, M. C. (1953). A new roundness scale for sedimentary particles. *Journal of Sedimentary Research*, *23*(2), 117–119. https://doi.org/10.1306/d4269567-2b26-11d7-8648000102c1865d

Reijmer, J. J. G. (2021). Marine carbonate factories: Review and update. *Sedimentology*, *68*(5), 1729–1796. https://doi.org/10.1111/sed.12878

Riazi, A., & Türker, U. (2019). The drag coefficient and settling velocity of natural sediment particles. *Computational Particle Mechanics*, *6*(3), 427–437. https://doi.org/10.1007/s40571-019-00223-6

Romanovskii, V. V. (1972). Experimental investigation of settling velocity of sediments. *Gosudarstvennyy Gidrologicheskiy Institut*, *191*, 111–136.

Rouse, H. (1949). *Elementary Mechanics of Fluids*. Wiley.

Schlager, W. (2003). Benthic carbonate factories of the Phanerozoic. *International Journal of Earth Sciences*, *92*(4), 445–464. https://doi.org/10.1007/s00531-003-0327-x

Schulz, E. F. (1954). *Effect of shape on the fall velocity of sand particles* [Master thesis]. Colorado Agricultural and Mechanical College.

Schulz, E. F., Wilde, R. H., & Albertson, M. L. (1954). *Influence of shape on the fall velocity of sedimentary particles* (MRD Sediment Series No. 5). Colorado Agricultural and Mechanical College & The Missouri River Division Corps of Engineers, U.S. Army; Mountain Scholar. https://hdl.handle.net/10217/184172

Slootman, A., de Kruijf, M., Glatz, G., Eggenhuisen, J. T., Jobe, Z. R., & Reijmer, J. J. G. (2026). Settling velocity of sediment grains, Part 2: Volume/Area ratio as descriptor of particle size and shape in sediment hydrodynamics. *Sedimentologika*, *4*(1). https://doi.org/10.57035/journals/sdk.2026.e41.2307

Slootman, A., de Kruijf, M., Glatz, G., Eggenhuisen, J. T., Zühlke, R., & Reijmer, J. J. G. (2023). Shape-dependent settling velocity of skeletal carbonate grains: Implications for calciturbidites. *Sedimentology*, *70*(6), 1683–1722. https://doi.org/10.1111/sed.13103

Smith, D. A., & Cheung, K. F. (2003). Settling Characteristics of Calcareous Sand. *Journal of Hydraulic Engineering*, *129*(6), 479–483. https://doi.org/10.1061/(ASCE)0733-9429(2003)129:6(479)

Southard, J. (Ed.). (2006). *Course Number 12.090: Introduction to Fluid Motions, Sediment Transport, and Current-Generated Sedimentary Structures*. Massachusetts Institute of Technology; OpenCourseWare. https://ocw.mit.edu/courses/12-090-introduction-to-fluid-motions-sediment-transport-and-current-generated-sedimentary-structures-fall-2006/

Stokes, G. G. (1850). On the Effect of the Internal Friction of Fluids on the Motion of Pendulums. *Transactions of the Cambridge Philosophical Society*, *IX*(II). https://ia600305.us.archive.org/20/items/b22464074/b22464074.pdf

Stringham, G. E., Simons, D. B., & Guy, H. P. (1969). *The behavior of large particles falling in quiescent liquids* (Professional Paper No. 562C). United States Geological Survey; USGS Publications Warehouse. https://doi.org/10.3133/pp562C

Swamee, P. K., & Ojha, C. S. P. (1991). Drag Coefficient and Fall Velocity of nonspherical particles. *Journal of Hydraulic Engineering*, *117*(5), 661–667. https://doi.org/10.1061/(ASCE)0733-9429(1991)117:5(660)

Vaz, M. F., & Fortes, M. A. (1988). Grain size distribution: The lognormal and the gamma distribution functions. *Scripta Metallurgica*, *22*(1), 35–40. https://doi.org/10.1016/S0036-9748(88)80302-8

Wadell, H. (1932). Volume, Shape, and Roundness of Rock Particles. *Journal of Geology*, *40*(5), 443–451. https://doi.org/10.1086/623964

Wadell, H. (1934). Some New Sedimentation Formulas. *Physics*, *5*(10), 281–291. https://doi.org/10.1063/1.1745211

Walsh, D. E., & Rao, P. D. (1988). *A study of factors suspected of influencing the settling velocity of fine gold particles* (Industry Research Laboratory Report No. 76; p. 43). University of Alaska Mineral Industry Research Laboratory. http://hdl.handle.net/11122/1133

Wang, Y., Zhou, L., Wu, Y., & Yang, Q. (2018). New simple correlation formula for the drag coefficient of calcareous sand particles of highly irregular shape. *Powder Technology*, *326*, 379–392. https://doi.org/10.1016/j.powtec.2017.12.004

Wentworth, C. K. (1922). A Scale of Grade and Class Terms for Clastic Sediments. *Journal of Geology*, *30*(5), 377–392. https://doi.org/10.1086/622910

Wilde, R. H. (1952). *Effects of shape on the fall-velocity of gravel-sized particles* [Master thesis, Colorado Agricultural and Mechanical College]. https://hdl.handle.net/10217/195976

Wu, W., & Wang, S. S. Y. (2006). Formulas for Sediment Porosity and Settling Velocity. *Journal of Hydraulic Engineering*, *132*(8), 858–862. https://doi.org/10.1061/(ASCE)0733-9429(2006)132:8(858)

Yordanova, E. K., & Hohenegger, J. (2007). Studies on settling, traction and entrainment of larger benthic foraminiferal tests: implications for accumulation in shallow marine sediments. *Sedimentology*, *54*(6), 1273–1306. https://doi.org/10.1111/j.1365-3091.2007.00881.x

Zhu, X., Zeng, Y., & Huai, W. (2017). Settling velocity of non-spherical hydrochorous seeds. *Advances in Water Resources*, *103*, 99–107. https://doi.org/10.1016/j.advwatres.2017.03.001

Zingg, T. (1935). Beitrag zur Schotteranalyse : die Schotteranalyse und ihre Anwendung auf die Glattalschotter. *Schweizerische Mineralogische Und Petrographische Mitteilungen*, *15*(1), 39–140. https://doi.org/10.5169/seals-15330